Microstructured Optical Fiber Made From Biodegradable and Biocompatible Poly(D,L-Lactic Acid) (PDLLA)

Agnieszka Gierej, Kurt Rochlitz, Adam Filipkowski, Ryszard Buczyński, Sandra Van Vlierberghe, Peter Dubruel, Hugo Thienpont, *Member, IEEE*, Thomas Geernaert, and Francis Berghmans, *Senior Member, IEEE*

***Abstract*—We have fabricated and characterized microstructured biodegradable and biocompatible polymer optical fibers using commercially available poly(D,L-lactic acid) (PDLLA). We first report on the preparation of the preforms by means of a novel technique based on transfer molding and on the fiber manufacturing using a regular heat-drawing process. We address the influence of the polymer processing on the decrease of the molar mass of PDLLA following the preform fabrication and the fiber optic drawing process. We investigate the in vitro degradation of the fabricated fibers in phosphate buffered saline (PBS) that reveals 21, 25 and 43% molar mass loss over a period of 105 days for fibers with diameters of 400, 200 and 100 μm, respectively. Cutback measurements return an attenuation coefficient as low as 0.065 dB/cm at 898 nm for a microstructured fiber with a diameter of 219 $\pm$ 27 μm. Due to immersion in PBS at 37 °C, the optical loss increases by 0.4 dB/cm at 950 nm after 6 h and by 0.8 dB/cm after 17 h.**

***Index Terms*—Biodegradable materials, microstructured polymer optical fiber, optical fibers, optical polymers, plastic optical fiber.**

Manuscript received 9 June 2022; revised 16 August 2022; accepted 6 September 2022. Date of publication 9 September 2022; date of current version 1 January 2023. This work was supported in part by the Research Foundation Flanders (FWO) Project G048915N 'Biodegradable Fiber Optic Technology for Biophotonic Applications' and Grant G0F6218N (EOS-convention 30467715, in part by the Interreg (NWE758, Fotonica pilootlijnen) Programme, and in part by the Vrije Universiteit Brussel through Industrial Research Fund (IOF) and the Methusalem- OZR programmes. Łukasiewicz Research Network - Institute of Microelectronics and Photonics was supported in part by the Project POIR.04.04.00-1C74/16 operated within the Foundation for Polish Science Team Programme and in part by the European Regional Development Fund under Smart Growth Operational Programme (SG OP), Priority Axis IV. *(Corresponding author: Agnieszka Gierej.)*

Agnieszka Gierej, Kurt Rochlitz, Hugo Thienpont, Thomas Geernaert, and Francis Berghmans are with the Department of Applied Physics and Photonics, Brussels Photonics (B-PHOT), Vrije Universiteit Brussel, B-1050 Brussels, Belgium (e-mail: agnieszka.gierej@vub.be; kurt.rochlitz@vub.be; hugo.thienpont@vub.be; thomas.geernaert@vub.be; francis.berghmans@vub.be).

Adam Filipkowski and Ryszard Buczyński are with the Department of Glass, Łukasiewicz Research Network - Institute of Microelectronics and Photonics, 02-668 Warsaw, Poland, and also with the Faculty of Physics, University of Warsaw (UW), 02-093 Warsaw, Poland (e-mail: adam.filipkowski@itme.edu.pl; ryszard.buczynski@fuw.edu.pl).

Sandra Van Vlierberghe is with the Department of Applied Physics and Photonics, Brussels Photonics (B-PHOT), Vrije Universiteit Brussel, B-1050 Brussels, Belgium, and also with the Department of Organic and Macromolecular Chemistry, Polymer Chemistry, Centre of Macromolecular Chemistry (CMaC), and Biomaterials Group (PBM), Ghent University, B-9000 Ghent, Belgium (e-mail: sandra.vanvlierberghe@ugent.be).

Peter Dubruel is with the Department of Organic and Macromolecular Chemistry, Polymer Chemistry, Centre of Macromolecular Chemistry (CMaC), and Biomaterials Group (PBM), Ghent University, B-9000 Ghent, Belgium (e-mail: peter.dubruel@ugent.be).

Color versions of one or more figures in this article are available at https://doi.org/10.1109/JLT.2022.3205451.

Digital Object Identifier 10.1109/JLT.2022.3205451

I. Introduction

BIOCOMPATIBLE and bioresorbable optical fibers carry potential for enhancing light-based medical diagnosis and treatment as they provide for the straightforward delivery of light from an optical source to target tissue using materials that do not harm and are not toxic to surrounding tissue, and that can be functionalized in view of a particular application scenario.

A recent state-of-the-art in the development of a biodegradable and implantable optical fibers has been given in [1]. Various transparent biomaterials have been employed to form such novel waveguides with various functionalities. A first yet rather unusual structured biodegradable polymer optical fiber made from cellulose has been proposed in 2007 already [2]. A. Dupuis, et al. reported on a thermally drawn double-core porous fiber made from cellulose butyrate (CB) tubes, with an inner cladding consisting of polydisperse hydroxypropyl cellulose powder (HPC) suspended in air. The cellulose tube could either be collapsed to create a solid core supporting light delivery or could remain open in view of supporting drug delivery. Despite the relatively high attenuation of around 1.1 dB/cm at 630 nm, this structured fiber allowed monitoring changes in transmission when its pores were filled with deionized water.

In the meantime, other types of specialty waveguides have been fabricated from biodegradable and biocompatible materials. A first class of materials includes bio-derived natural polymers, such as silk [3], [4], [5], genetically engineered recombinant silk [6], cellulose [2], [7], [8], [9] agarose [10], [11], and gelatin [12]. A second class involves synthetic polymer hydrogels, i.e., polyethylene glycol (PEG) [13], [14], alginate-polyacrylamide [15], poly(acrylamide-co-poly (ethylene glycol) diacrylate) (p(AM-co-PEGDA)) [16], synthetic polyesters such as poly(L-lactic acid) (PLLA) [17], [18], citrate-based polymeric elastomers POC-POMC [19], poly(D,L-lactic acid) (PDLLA) [20], and poly(D,L-lactic-co-glycolic acid) (PDLGA) [21], [22].

In addition, inorganic glass-based materials including calcium phosphate [23], [24], [25], [26], have been used to fabricate optical fibers, as well as other various hybrid materials to form multifunctional fibers [27], [28], [29].

The examples listed above are either unclad – for a vast majority – or occasionally step-index type optical fibers. Microstructured optical fibers made from biocompatible materials have only been proposed by S. Shadman, et al. [22] These came in different shapes i.e., rectangular, cylindrical and core-shell, and they were fabricated by means of thermal drawing from preforms consisting of poly(D,L-lactic-co-glycolic acid) (PDLGA) combined with poly(methyl methacrylate) (PMMA) and poly-ε-caprolactone (PCL). The optical characteristics of these microstructured fibers, however, were not reported. Note that bioresorbable phosphate glass was also used for manufacturing microstructured fibers using a stack-and-draw technique [25]. Structured preforms were prepared by stacking extruded capillaries within a tube, and were then heat-drawn into a fiber [30]. The authors demonstrated light guidance at 1300 nm, but without detailing the optical characteristics. E. Fujiwara et al. [11] fabricated structured agarose optical fibers consisting of a solid core surrounded by one ring of six air holes. The fiber was prepared by directly pouring solubilized agarose into a glass mold with an inner diameter of 3 mm consisting of six internal rods with a diameter of 0.5 mm. The agarose-based fiber featured a relatively high attenuation of 3.23 dB/cm at 633 nm.

Given the above, we can fairly state that only very limited efforts have been conducted for developing biocompatible and resorbable microstructured optical fibers and that the fibers obtained thus far feature a high attenuation, which essentially limits their potential for application, e.g., for photodynamic therapy, in-vivo light-induced drug release, or in-vivo biosensing. The concept of guiding light using a microstructured optical fiber is nevertheless well established and has been widely explored in both silica glass fibers [31], [32], [33] and regular polymer optical fibers [34], [35], [36]. Well-known advantages include the design flexibility and the option to tailor the optical guidance properties in view of achieving application-specific characteristics as well as the possibility to fabricate the fiber from a single material. For POFs in general, microstructuring may allow achieving singlemode guidance, which is typically difficult to obtain with a step-index structure in polymers given the higher refractive index of polymers compared to glass and given the wavelength range in which POFs typically operate. For our biocompatible and biodegradable fibres in particular, an additional advantage may come from the ability to use the airholes of the microstructure as ducts for drugs or capillaries carrying analytes that can interact with light in a controllable manner in view of enabling new phototherapy or biosensing applications. Furthermore, we anticipated that working with a single biopolymer instead of two would facilitate the control over the fiber drawing process given that potential incompatibilities between different biopolymers can be avoided.

The above prompted us to investigate the fabrication and to characterize microstructured biocompatible and biodegradable polymer optical fiber (mbioPOF) developed from a U.S. FDA-regulated commercially available polyester PDLLA [37]. The choice of this polymer is based on our previous work on unclad PDLLA [20] and step-index PDLGA-PDLLA [21] optical fibers that were fabricated with a standard heat-drawing process and which revealed low attenuation and satisfactory thermomechanical stability with a potentially tunable degradation time.

Our paper is structured as follows. Section II describes the whole fabrication process starting from the fiber design, going through the preform fabrication, and ending with the actual mbioPOF drawing. In Section III, we shortly report on the influence of the fabrication process on the thermo-mechanical and physico-chemical properties of the polymer by comparing the molar mass of the granulate, the preforms and the eventual fibers. Section IV provides a detailed optical characterization of two batches of fabricated mbioPOFs and reports on the mode confinement and on the attenuation coefficient measured by a conventional cutback method. In Section V, we describe the *in vitro* degradation of our mbioPOFs over a period of 3 months and in Section VI, we report on the evolution of the optical loss in mbioPOF as a function of time following immersion in phosphate-buffered saline. We close our manuscript with Section VII, including a summary of our research supplemented with perspectives for further research.

II. Fabrication

A. Fiber Design

Our base material is PDLLA (PURASORB PDL 20) with an inherent viscosity of 2.0 dl/g in the form of granulate from Corbion Purac Biomaterials [38]. We have already reported on the chemical and optical characteristics of this starting material in [20].

To design our mbioPOF and in view of calculating the confinement loss for various lay-outs of the fiber cross-section, we have first carried out simulations using the commercially available MODE waveguide design software from Ansys/Lumerical, Inc. [39] to investigate the confinement loss of our mbioPOF structure. Our main objective was to identify a design of the microstructure in the cross-section of the fiber that provides for a confinement loss that is smaller than the material loss reported for unclad PDLLA fiber, i.e., 0.16 dB/cm at 650 nm [20]. Even though the lowest loss for unclad PDLLA was 0.11 dB/cm at 772 nm [20], we selected the loss of 0.16 dB/cm at 650 nm as a reference for the simulations, because we have previously assessed the refractive index of PDLLA at this wavelength using an Anton Paar Abbemat MW refractometer. Knowledge of the exact value of the refractive index is indeed mandatory for conducting the simulations using Ansys/Lumerical Mode Solutions software. The purpose of the simulations was therefore solely to compare the order of magnitude of the confinement loss for various airhole sizes (d) and pitch values (Λ) that provide for a sufficiently low confinement loss. We eventually selected a mbioPOF design with a high air filling factor (d/Λ) of around 0.8 to ensure light confinement within the core region. This can be achieved using an airhole lattice with a limited number of airhole rings and a larger airhole size, which in its turn facilitates the preform fabrication. The fiber design is highly multimode. The simulated mode field distributions of the fundamental mode

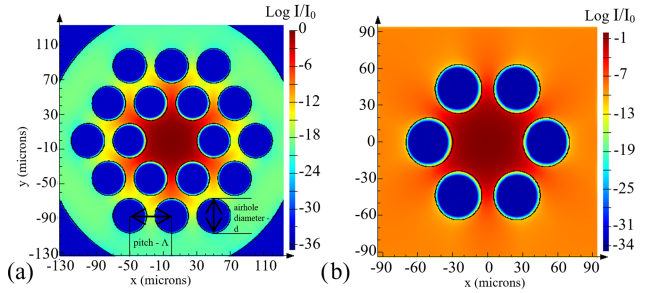

Fig. 1. Mode field distribution of the fundamental mode (a) in an optical fiber holding an array with two rings of airholes, with an effective refractive index 1.45398 and yielding a confinement loss of around 10^{-15} dB/cm at 650 nm. The pitch (Λ), and airhole diameter (d) are indicated, (b) in an optical fiber holding an array with one ring of airholes, with an effective refractive index 1.45398 and yielding a confinement loss of around 10^{-7} dB/cm at 650 nm. The color scale shows the energy distribution in a logarithmic scale.

(shown in Fig. 1) and the second order modes for an array with two rings of 18 airholes, d/Λ = 0.8, pitch Λ = 50 μm, and airhole diameter d = 40 μm, returns a confinement loss in the range of 10^{-15} dB/cm at 650 nm, while the higher order modes are guided with a confinement loss of around 10^{-8} dB/cm. We also performed a simulation of the confinement loss at 650 nm on the hexagonal lattice holding one ring of 6 airholes. The modal field distribution of the fundamental mode shows a confinement loss of around 10^{-7} dB/cm, while the second order modes return a confinement loss of around 10^{-6} dB/cm, which are negligible values compared to the overall propagation loss. For both the single and double ring structure, the highest confinement loss values are of the order of 10^{-2} dB/cm, which is still well below the attenuation due to bulk PDLLA absorption at 650 nm. Although our multimode mbioPOF guides thousands of modes of which we did not study the loss values, we can safely assume that given our design and assuming that this design can be successfully fabricated, the confinement loss should not contribute significantly to the overall propagation loss.

B. Preform Fabrication

To fabricate a structured preform from PDLLA, we designed and developed a dedicated molding system in the form of an add-on to our in-house Jenoptik HEX04 hot embossing system. This add-on essentially transforms the compression-molding system into a transfer-molding system and provides for an entirely novel and highly controllable microstructured POF preform fabrication method. In essence, this preform fabrication method is not limited to the use of biocompatible polymers but may also be applied for fabricating preforms from polymers that are regularly used in the fabrication of POFs, such as PMMA. The add-on system is illustrated in Fig. 2(a) and (e).

The polymer granulates are initially inserted in a steel cylinder and closed with a plunger. The cylinder was heated up both by the bottom plate of the HEX04 system, and by a supplemental heating band that provides for more uniform heating of the polymer. The steel plunger fits into the heated cylinder and is pressed downwards with a force supplied by the HEX04 system. Once the polymer was heated up above its glass transition temperature (T_g), the viscous mass was forced to flow from the cylinder

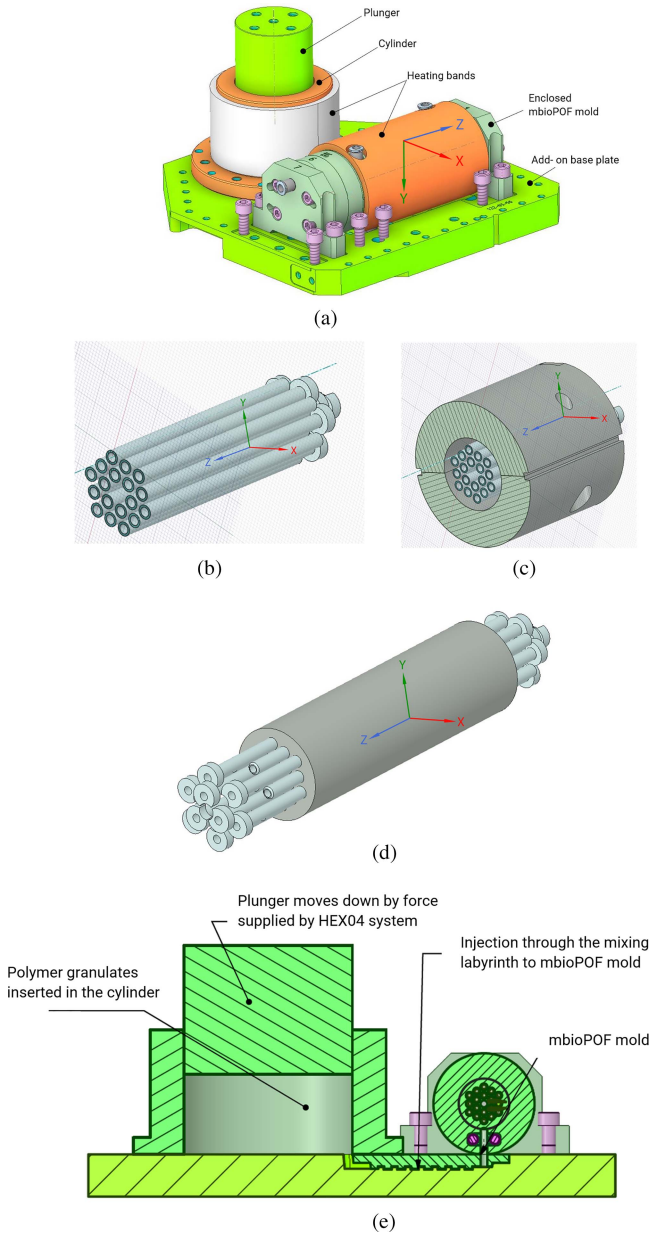

Fig. 2. Illustration of the transfer molding system used to fabricate mbioPOF preforms, (a) the 3D CAD model of the add-on with all its parts labeled, (b) the set of 18 aligned hollow pins that essentially form the array of airholes also represented in Fig. 1. (a), (c) the set of hollow pins installed within the outer mbioPOF mould that opens along the z-axis, (d) the set of hollow pins now surrounded by the polymer preform (in grey), (e) 2D cross-section of the model with description of the main components.

through the mixing labyrinth that ensures the homogeneity of the softened polymer mass before it accesses the dedicated structured mold.

Using the system described above, we have manufactured one mbioPOF preform with one ring of 6 holes (labeled as PR1, see also Fig. 1(b) for an illustration of the design of the cross-section of the preform) and two mbioPOFs preforms with two rings of 18 holes (labeled as PR2a and PR2b, see also Fig. 1(a) for illustration). The transfer molding of PR1 was conducted with a force of around 90 kN, which corresponds to a pressure of 5.37 MPa given the compressed cylinder area. Prior

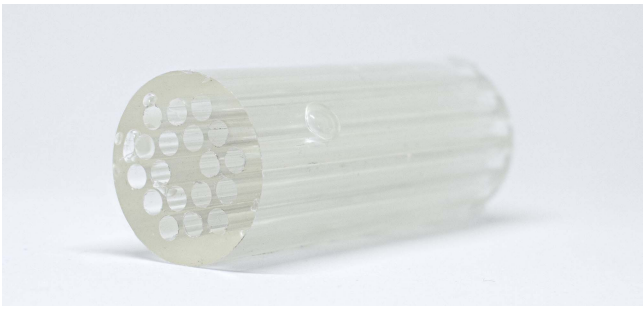

Fig. 3. Photograph of structured preform (PR2b) with two rings of airholes (18 holes in total) and a length of 75 mm.

to that, PDLLA granulates (about 60 g) were kept in vacuum and preheated for 3 h at 190 °C. An additional ring-shaped heating band that keeps the temperature at 150 °C was clamped around the mbioPOF mold to ensure that the molten polymer would not solidify too quickly. The transfer process of PR1 lasted about 20 min and the polymer flowed at a volumetric rate of 3.3 cm^3/min. Once the polymer was injected, the mold was forced to cool down by means of an airflow directed inside the airholes until the mold reached a temperature below 40 °C, which is below the T_g of PDLLA granulates. Along the process, the material experiences thermal stress caused by differences in thermal expansion between the mold and the polymer, which in its turn leads to difficulties to demold the preform. Although the pins and the internal part of the stainless-steel mold were coated with PTFE (Teflon) and Diamond-Like Carbon (DLC), manual demolding of the pins by simply pulling them out of the preform appeared impossible. We have therefore manufactured a dedicated demolding tool to apply an unscrewing motion to the pins, which allowed removing them one by one from the preform. In view of facilitating the demolding of the preform, we also investigated transfer molding at lower temperatures, i.e., 120–140 °C, at which the drawing of PDLLA optical fibers has been previously demonstrated. This allowed obtaining preforms PR2a and PR2b, which were manufactured by first preheating the polymer granulates at 135 °C for 100 minutes and then applying a maximum force of 90 kN at 140 °C. The temperature of the heated band surrounding the mbioPOF preform mold was set at 120 °C to prevent polymer solidification, given that the polymer injection lasts for about 190 minutes. After successful polymer injection, we cooled down the preform mold to 30 °C using an airflow. Removal of the pins from preforms PR2a and PR2b was much easier and achieved with the same demolding tool by "unscrewing" the pins for only half of their length followed by a simple manual extraction. Preform PR2a contained multiple small bubbles that most likely result from the compression-decompression cycle carried out on the HEX04. However, this PR2a preform remained free of contamination, in contrast to preform PR2b. Said contamination most likely happened during the material insertion due to impurities that remained in the mold following incomplete cleaning. Fig. 3 shows a photograph of the mbioPOF preform PR2b.

TABLE I
PARAMETERS USED DURING HEAT-DRAWING OF MBIOPOFS

	PR1	PR2a	PR2b
Preform length [cm]	75	45	75
Preheating temperature [°C] for 30 min	120	120	130
Initial weight [g]	220	80	172
Drawing temperature [°C] range	155-146	159-150	150-145
Pressure of N_2 flow to the preform [mbar]	20-25	50	1-4
Feeding [mm/min]	0.005-0.001	0.01-0.005	0.001
Drawing [m/min]	4-5	2-5	22.5-17.3
Fiber diameter [μm]	500-150	1000-270	190-100

C. Fiber Drawing

Following the fabrication of the preforms, we used regular heat-drawing to obtain three batches of mbioPOFs labeled M1 (from preform PR1), M2a (from preform PR2a) and M2b (from preform PR2b). In total, we produced a few hundreds of meters of mbioPOF, indicating that long lengths can readily be obtained and hence that the fabrication method can be used to fabricate such fibers in large volumes.

The drawing temperature of the structured preforms was set empirically by increasing the temperature up to the point where the polymer started softening and the preform began to form a neck-down shape. For initiating the drawing, we clamped a small weight to the bottom of the preform. To avoid oxidation of the polymer preforms, we flushed the furnace with a constant N_2 flow of 200 l/h. Additionally, we also directed a N_2 flow of 50 l/h inside the preform to allow for a better control over the airhole dimensions during the fiber drawing process. The N_2 flow through the drawing section of the furnace should be further optimized to prevent highly turbulent flow patterns that can result in either hole collapse or expansion depending on the drawing speed, the drawn fiber diameter and the drawing temperature. Table I summarizes the heat-drawing parameters for each preform.

III. CHEMICAL CHARACTERIZATION

To determine the influence of the processing on the thermo-mechanical and physico-chemical properties of the polymer, we have conducted size-exclusion chromatography (SEC) analysis on a Waters GPC Alliance 2695 device with respect to PS reference standard of both the fabricated structured preforms and the eventual mbioPOFs. Fig. 4 shows the weight averaged molar mass, Mw, of PDLLA granulate, of the three types of preforms (PR1, PR2a and PR2b), and of two mbioPOFs (one ring M1 and two rings M2b). We observe a 38% decrease of the molar mass for preform PR1 with respect to the PDLLA granulates, and a 21% and 25% decrease for preforms PR2a and PR2b, respectively. The molar mass differences between these samples stem from the altered temperatures applied to PDLLA during the transfer molding. Note indeed that PR2a and PR2b were fabricated at 140 °C, while PR1 was fabricated at 190 °C, which caused the larger thermal degradation of PR1.

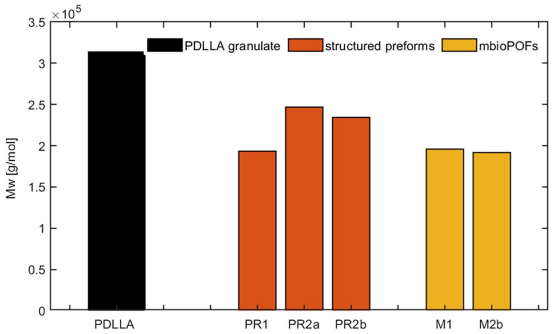

Fig. 4. Mw values for PDLLA granulates, three types of preforms and two microstructured fibers.

IV. Optical Characterization

A. Mode Confinement in the Fabricated MbioPOFs

The heat-drawing process induced deviations in shape and size from the initially intended airhole pattern in the preforms. Fig. 5 shows scanning electron microscope (SEM) images of the facets of three batches of mbioPOFs.

To understand how the airhole deformation impacts the optical waveguiding properties, we have computed the confinement loss using the MODE simulator of Λnsys/Lumerical, Inc. for the actual airhole pattern in the as-built mbioPOFs. These patterns, and more specifically, the edges of the airholes that define the microstructure, are obtained by image processing of the SEM micrographs of the mbioPOF cross-sections.

In our initial design, the hole diameter (d) was equal to 40 μm and the pitch (Λ) was 50 μm, which gives an air filling factor (d/Λ) of 0.8. For fiber M1 with an outer diameter of around 260 μm, the six holes featured various shapes and diameters between 18 and 22 μm, which is 55%–45% smaller than anticipated. The pitch is 33−37 μm, which is 34%−26% smaller than in the initial design. The higher order modes in fiber M1 therefore leak out easily: the high confinement loss indeed indicates that these modes radiate out of the fiber core. The M2a mbioPOF with around 300 μm outer diameter holds eighteen holes with various shapes and diameters and hence it is not straightforward to estimate the air filling factor.

The confinement loss for the fundamental mode is five orders of magnitude higher than the value given by the initial design. The higher order modes partially leak out from the fiber core to the outer ring, but their confinement loss is still below the material loss value. mbioPOF M2b with an outer diameter of 135 μm features the most dramatic distortion: the pattern of the microstructure is entirely deformed and the airholes come with various shapes and sizes. Nevertheless, owing to the airhole expansion and the very short distance between the adjacent airhole centers, this microstructure demonstrates excellent mode confinement. Fig. 6 shows the calculated spatial intensity profile of the fundamental mode and the second higher order mode, respectively. The confinement loss of the fundamental mode is of the same order of magnitude (10^{-15} dB/cm) as the value calculated in the mbioPOF design.

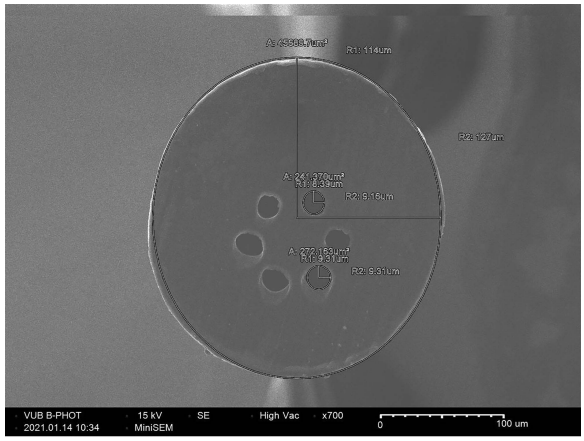

(a)

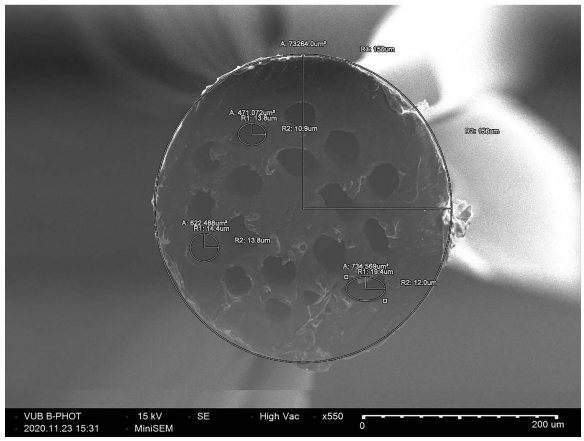

(b)

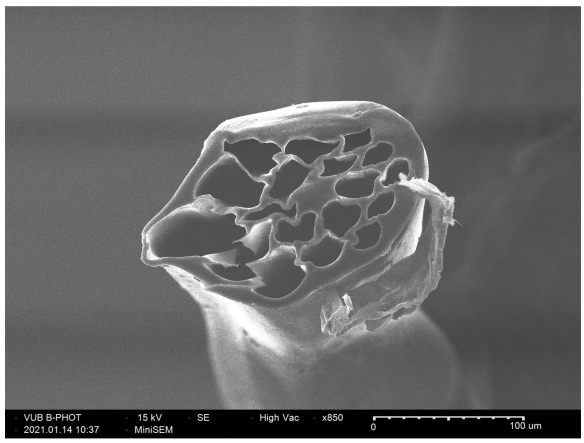

(c)

Fig. 5. SEM image of the end-facet of mbioPOFs: (a) M1 with one ring of airholes, cross-sectional radii of 114 and 127 μm, and airhole radius of around 9 μm, (b) M2a with two rings of airholes, cross-sectional radii of 150 μm and 156 μm, and holes radii varying from 10 to 19 μm, (c) M2b with two rings of airholes. The fiber diameter is around 135 μm.

To demonstrate the guiding capabilities of the fabricated mbioPOFs, we launched optical power emitted by a HeNe-laser into the fibers, and we recorded the far-field power exiting from their end-facet. Because of the limited mode confinement,

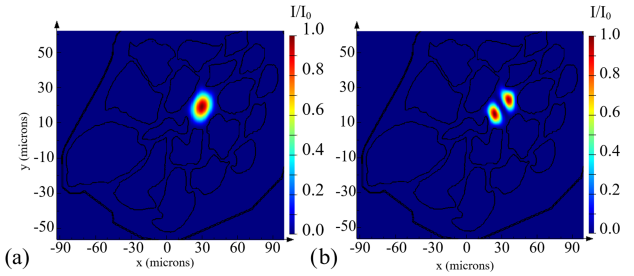

Fig. 6. Mode field distribution of (a) the fundamental mode in fiber M2b with a confinement loss of $1.57{*}10^{-15}$ dB/cm at 650 nm, effective refractive index 1.45384, (b) a higher order mode in fiber M2b with a confinement loss of $1.93{*}10^{-14}$ dB/cm at 650 nm, effective refractive index 1.45369. The colors scale shows the energy distribution in a linear scale.

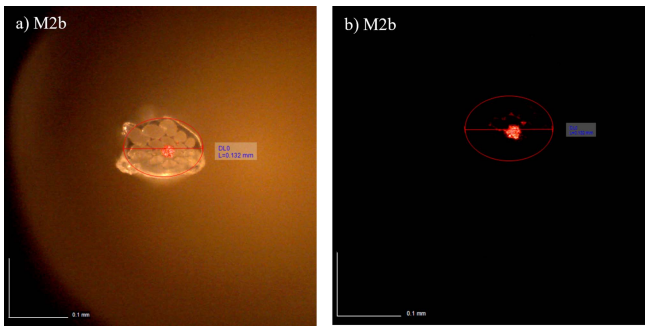

Fig. 7. Mode confinement in the solid core of mbioPOF M2b, (a) M2b fiber with light propagating in its core and indirect outer illumination, (b) M2b fiber with light propagating in its core, kept in darkness, clearly revealing the mode confinement within the core. The red line indicates the elliptical shape with major axis L.

we immersed the total fiber length in an oil with a higher refractive index ($n = 1.48$ at 650 nm), with the intention to eliminate weakly guided cladding modes. Although these fibers do not exhibit strong mode confinement in the core area, higher order modes are guided along the fiber despite bending and immersion in higher refractive index oil. This is not the case for unclad PDLLA fiber that we have previously fabricated and characterized in [20], as immersing it in a liquid with a refractive index higher than PDLLA leads to full decay of the electromagnetic field outside of the waveguide. Fig. 7 shows the cross-section of the end-facet of mbioPOF M2b, with an elliptical shape and a major axis of around 132 μm, and clearly demonstrates the modal field confinement in the core of the fiber. Whilst light guidance has previously been shown in a structured yet incompletely characterized bioresorbable phosphate glass-based fiber [25] and in a structured agarose-based fiber [11] with feature sizes in the millimeter range, our results represent the first demonstration ever of microstructure-based light guidance in commercially available and synthetic polymer-based fully-fledged microstructured optical fiber.

B. Attenuation

We measured the spectral attenuation of the three types of mbioPOFs by means of cutback measurements and using a broadband Laser-Driven Light Source Model EQ-99X-FC

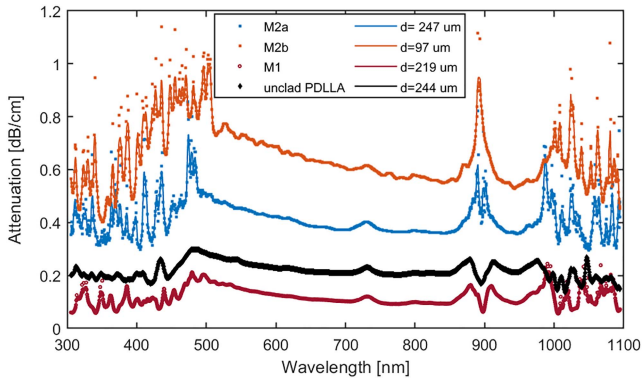

Fig. 8. Spectral attenuation curves for measured mbioPOFs and unclad PDLLA fiber. d indicates the average outer diameter.

LDLS^{TM} and an AvaSpec2048 spectrum analyzer. We cut the fiber ends using a microtome blade on a hot plate kept at around 27–30 °C. Cutback measurements were carried out in air and the fibers were not immersed in any liquid during the study. The bare microstructured fiber ends were temporarily fixed into a Ø 340–280 μm bore SS Ferrule for multimode SMA905 connectors and connected to optical fibers leading to the source and to the detector with SMA mating sleeves. We measured two M2 fibers with different average diameters of M2a = 247 ± 21 μm and M2b = 97 ± 7 μm, as well as M1 fiber with a diameter of 219 ± 27 μm. We have also carried out a cutback measurement on a previous unclad PDLLA fiber with a comparable diameter of 244 ± 44 μm [20]. All the spectral attenuation plots of the mbioPOFs and unclad PDLLA are shown in Fig. 8. The lowest attenuation of 0.065 dB/cm was found for M1 at 898 nm, which – to the best of our knowledge – is the lowest optical loss value reported for bioPOF. M1 fiber also features low loss of around 0.1 dB/cm in the 750–850 nm region.

The M1 mbioPOF features the lowest attenuation of all mbioPOFs that we have fabricated. This may indicate that the quality of the preform material affected the transmission more than the fiber design. Both M2 preforms contained small bubbles and imperfections along the preform length, which may have increased scattering leading to higher optical loss. Although mbioPOF M2b features clear mode confinement in the core, it returns the highest attenuation value, which is most likely due to scattering and contamination of the polymer granulates during the material insertion. We believe that the recorded attenuation values therefore stem from the purity of the material following the preform preparation and can be further decreased by means of light guidance strictly confined to the mbioPOF core.

Note that the lowest loss appears around 900 nm, where we observe a split within a third overtone of the C-H stretching [40] absorbance band, both in mbioPOF M1 and in unclad PDLLA fiber. This phenomenon is also present in mbioPOF M2, but to a lesser extent, as shown in Fig. 9. Considering that we did not observe this local minimum at 900 nm in the attenuation spectrum of bulk PDLLA material, we conjecture that this phenomenon is caused by the heat-drawing process. Heat-drawing to some extent aligns the amorphous polymer chains, and the spectral

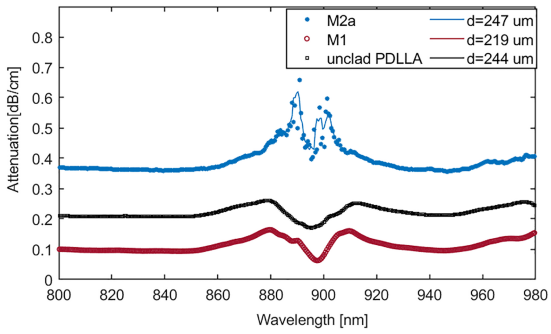

Fig. 9. Spectral attenuation in the near infrared (NIR) region of M1, M2a and unclad PDLLA fibers with indicated diameters.

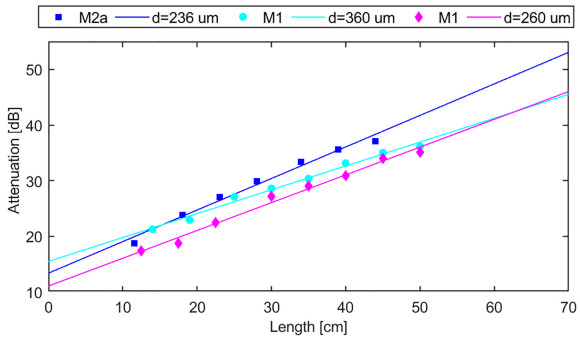

Fig. 10. Cutback measurement results at 1580 nm for mbioPOFs M2a and M1. The solid lines are the linear regressions, the slope of which returns the attenuation coefficient in dB/cm. $R^2 = 0.983$ for M2a, $R^2 = 0.988$ for M1, d = 360 μm, $R^2 = 0.988$ for M1, d = 260 μm.

band split may arise as a result of the lateral interactions between the polymer chains. According to E. Meaurio et al. [41], this could be explained in terms of carbonyl−carbonyl intramolecular coupling or specific interactions such as dipole−dipole forces between polar groups, or C−H···O hydrogen bonding, or interactions involving the newly formed -COOH and -OH functionalities resulting from hydrolysis of the ester moieties, although confirming this requires further investigations.

Finally, we also conducted cutback measurements on mbioPOFs M1 and M2a at 1580 nm using a TSL-710 Santec tunable laser and a Newport 918D-IR-OD3R Germanium Photodetector. The attenuation for M1, d = 260 μm, equals 0.50 dB/cm and for M1, d = 360 μm we measure a value of 0.43 dB/cm. Fiber M2a features an attenuation of 0.57 dB/cm at 1580 nm which is shown in Fig. 10. This analysis indicates the presence of a relatively low loss window for mbioPOFs in the L-band, which is typically employed as a second primary wavelength band for optical communications with silica optical fibers. The loss at the same wavelength given by unclad PDLLA fiber were 1.1 dB/cm reported in [20], while for PMMA around 1.36 dB/cm [42]. It is worth noting that the relatively low loss window of PDLLA in the L-band may be interesting for example in view of creating fiber optic sensors in this wavelength range by means of the photo-inscription of fiber Bragg gratings, should PDLLA allow for that.

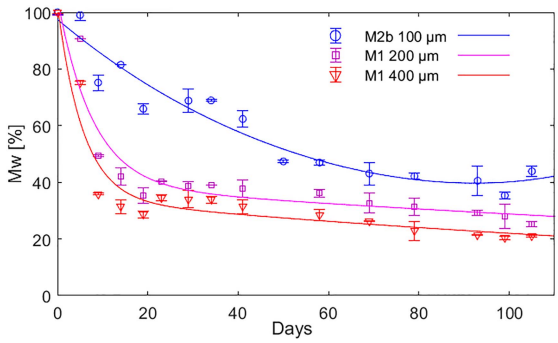

Fig. 11. Mw percentage of mbioPOFs incubated at 37 °C in PBS as a function of time. Error bars represent the standard deviation for each sample that was measured twice, and the solid line represents the exponential fit.

V. Degradation in PBS

Given that our mbioPOFs are meant to be biocompatible and degradable, we have investigated the degradation of mbioPOFs in a simulated biological environment. To do so, we immersed short fiber portions from two fabrication batches with various diameters (M2b 100 μm, M1 200 μm, and M1 400 μm) in sterilized phosphate-buffered saline (PBS) (0.1 M, pH = 7.4), at 37°C for a period of 105 days. We analyzed the weight averaged molar mass (Mw) of the mbioPOFs using SEC on the Waters GPC Alliance 2695 device every 4-7 days during the total immersion time. Each sample was measured twice and the averaged Mw with a standard deviation for these two datasets were fit to the model that has been previously applied for the hydrolysis of polyester-based samples [21], [43], which is relying on first order kinetics, i.e., a sum of an initially fast and a delayed exponential decay and which is given by (1).

$$Mw\,(t) \;=\; Mw_{01}exp(-k_1 t) + Mw_{02}exp(-k_2 t) \qquad (1)$$

Mw_{01} is the molecular weight before hydrolysis, Mw_{02} is the molecular weight at the start of the second hydrolysis stage and $-k_1$ and $-k_2$ are the kinetic constant rates for each degradation stage.

Fig. 11 shows the degradation of mbioPOFs with one ring (M1) and two rings (M2b) of airholes. M1 fibers clearly reveal two stages with fast and slow degradation rates. On the other hand, fiber M2b features a considerably different degradation profile. The fit uncertainty with the sum of two exponential degradation terms is $R^2 = 0.9356$ and $R^2 = 0.9173$ for M1 400 μm and M1 200 μm, and $R^2 = 0.9331$ for M2b 100 μm, respectively.

The degradation rate of mbioPOFs depends on their diameter, similarly to what was already shown with unclad PDLLA fibers in [20]. The fastest degradation rate occurs for the thicker fibers, which supports that the degradation in the bulk occurs faster than at the surface of the polyester samples and that the accelerated degradation takes place in the center due to a negative gradient of the penetrating water concentrations from the surface to the sample's center [44] that stems from the catalytic effect of the carboxylic acid groups.

After a first week of incubation, we observed that the polymer changed from transparent to white and that 400 μm diameter fibers got slightly swollen due to some water uptake, whilst 100 μm diameter fibers did not swell but got randomly coiled. Their mechanical integrity, however, was maintained. Following the first 9 days of incubation, we noted a significant decrease of the molar mass down to 36% and 49% of the initial values, which happened with an initial kinetic rate of 0.179 day^{-1} (257.7 min^{-1}) and 0.129 day^{-1} (186.5 min^{-1}) for the 400 μm and 200 μm diameter fibers M1, respectively. We recorded a significantly slower initial kinetic rate of 0.014 day^{-1} (20.6 min^{-1}) with a molar mass reduction of only 25% for fiber M2b with a diameter of 100 μm. We can therefore conclude that for M1 fibers, the degradation rate starts with a substantial decrease of the molar mass corresponding to rapid water penetration and initiation of polymer backbone rupture generating hydroxyl and carboxyl acid end groups. After approximately 20 days, the phase of the fast molar mass decay has ended and is followed by a slower hydrolysis of polyester molecular chains with a decelerated kinetic rate of 0.0044 day^{-1} (6.3 min^{-1}) and 0.0029 day^{-1} (4.3 min^{-1}) for M1 400 μm and M1 200 μm, respectively, that lasts until the end of the study, and results in a Mw decrease down to around 21% and 25% for M1 400 μm and M1 200 μm, respectively, after 105 days of incubation. Note that we have previously registered a similar value of the kinetic rate of 0.171 day^{-1} (246.2 min^{-1}) corresponding to the "faster" degradation phase for 600 μm unclad PDLLA bioPOF [21]. However, the following "slower" degradation phase with a kinetic rate of 0.0154 day^{-1} (22.2 min^{-1}) was 4-5 times faster for unclad PDLLA bioPOF than for M1 mbioPOF. This most likely stems from differences in fiber thicknesses, and from the presence of capillaries in the mbioPOFs. Additionally, the remaining molar mass of the 200 μm M1 mbioPOF was 4% higher than the remaining molar mass value given by unclad PDLLA fiber of the same diameter after 100 days of incubation which was reported in [20]. This demonstrates that the microstructured fibers are highly permeable due to the presence of airhole channels along their structure and therefore do not readily accumulate PBS like solid unclad PDLLA fibers do, which in its turn leads to a lower catalytic effect of the generated carboxylic acid groups upon bulk degradation, and which ultimately results in a slower kinetic rate during the second degradation phase. The degradation process of 100 μm diameter M2b fibers is however not typical for a polyester and occurs with a significantly slower rate than its higher diameter counterparts M1 200 μm and 400 μm, for which the initial kinetic rate is around 40 times faster than the secondary kinetic rate. For M2b fiber with a 100 μm diameter, there are not clearly distinguishable consecutive faster and slower kinetic rates. Instead, these kinetic rates are in the same range and equal to 0.014 day^{-1} (20.6 min^{-1}) and 0.026 day^{-1} (37.6 min^{-1}), respectively. This stems from the fact that we do not only deal with thinner fibers but also with more hollow structures. Given that the fiber is more porous, the acidic by-products of the hydrolysis breakdown cannot be easily trapped and kept within the very small fiber core (diameter of around 20 μm) and capillaries are readily flushed with saline solution, which facilitates the removal of acidic by-products. Consequently, we do not register two distinct stages of degradation, although the greatest decrease of the molar mass is still observed in the first 50 days of incubation due to the initial penetration of water molecules into the core. After the 105th day, the remaining molar mass of M2b samples was still around 43% of the initial value.

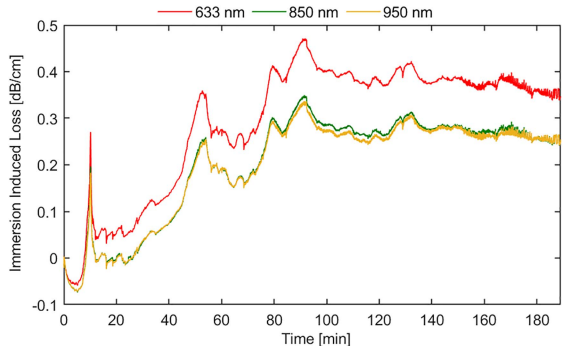

Fig. 12. Immersion Induced Loss (IIL) at three wavelengths for mbioPOF M1 immersed in PBS at 37 °C as a function of time in the first 3 hours after immersion.

Considering the dependency of the degradation rate on the sample thickness but also on the porosity, we are convinced that the PDLLA-based mbioPOF can be further optimized in terms of dimensions and structure, in view of matching a desired degradation profile for a targeted medical application.

VI. Immersion Induced Optical Loss

One of the typical ultimate purposes of any biodegradable and biocompatible POF would be to serve as an implantable optical fiber. We therefore also evaluated the optical loss in these fibers following immersion in PBS at 37 °C, pH = 7.4. To do so, we coupled broadband light from a Laser-Driven Light Source Model EQ-99X-FC LDLS^{TM} into a portion of M1 fiber section and we monitored the power output using an AvaSpec2048 spectrum analyzer. The Immersion Induced Loss (IIL) is defined by (2):

$$IIL = \frac{10}{L} * \log_{10} \frac{P(t=0)}{P(t)} \tag{2}$$

where P is the measured optical power exiting the fiber, t is the time and L is the length of the immersed fiber portion. The immersed fiber portion had a length of about 23 cm, and the total fiber length was 160 cm with an average diameter of 225 $\pm$ 29 μm. The fiber was kept straight under low tension during the experiment to prevent bending, which may cause additional optical loss.

Fig. 12 shows the IIL values at three selected wavelengths, i.e., 633, 850 and 950 nm, for mbioPOF M1 as a function of immersion time during the first three hours of immersion. At the start of the experiment, we observe an immediate, but short lasting (6 minutes) IIL decrease to -0.07 dB/cm at 850 and 950 nm and to -0.05 dB/cm at 633 nm due to initial water penetration to mbioPOF. The ILL decrease is presumably due to an increased number of guided modes because of the surrounding aqueous medium with lower refractive index and a reduced

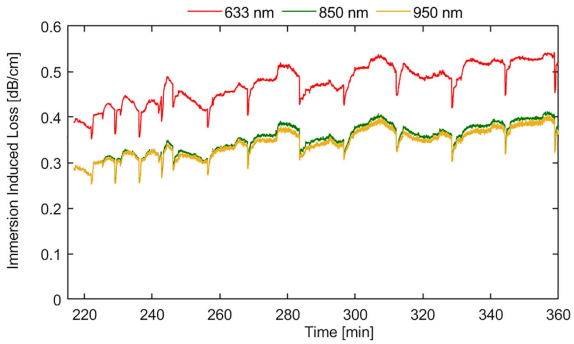

Fig. 13. Immersion Induced Loss (IIL) at three wavelengths for mbioPOF M1 immersed in PBS at 37 °C as a function of time, until the 6th hour of immersion.

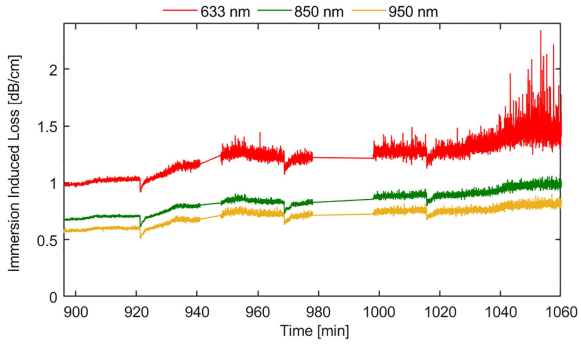

Fig. 14. Immersion Induced Loss (IIL) at three wavelengths of mbioPOF M1 immersed in PBS at 37 °C as a function of time. From the 15th hour of immersion until 17 hours and 40 min.

scattering due to the watered core-cladding interface. We have also previously observed this phenomenon for SI bioPOF in [21]. Next, we notice a temporary but high ILL increase between 0.2–0.3 dB/cm, after which the ILL drops to around 0 dB/cm at 850 and 950 nm, and 0.04–0.07 dB/cm at 633 nm for about 15 minutes. The absence of any additional loss in those 15 minutes is in accordance with the previously demonstrated ILL for unclad PDLLA and SI bioPOF. Subsequently, we observe a loss increase from 0 to around 0.35 dB/cm at 633 nm and to 0.25 dB/cm at 850 and 950 nm in a time span of 20 minutes followed by a loss decrease down to 0.27 dB/cm at 633 nm and 0.18 dB/cm at 850 and 950 nm for another 20 minutes before the next ILL increase. The reason of this instability in the recorded power and the rise and falls of the ILL is most likely due to the turbulent flow of PBS, which starts entering the capillaries of the mbioPOF and infiltrating the holey cladding. After 3 hours of immersion, the optical loss at 850 and 950 nm is 0.26 dB/cm, and up to 0.36 dB/cm at 633 nm. This is a significantly lower loss and a much more extended working time than these previously observed for both unclad PDLLA fiber and SI bioPOF, for which we registered an additional optical loss of around of 1-2 dB/cm after the first hour of immersion [20], [21].

Fig. 13 shows the ILL for mbioPOF M1 between the 3rd and 6th hour of immersion. In this period, the ILL increases from 0.4 to 0.55 dB/cm at 633 nm, and from 0.28 to 0.41 dB/cm at 850 and 950 nm. The ILL variations are less noticeable than in the first 3 hours. This can be attributed to increased infiltration of PBS and filling of the mbioPOF capillaries. However, since the solid core did not yet accumulate PBS with the terminal carboxyl acid formed upon hydrolysis, the hydrolysis itself is delayed, and the included loss increases at a much slower rate than for example in unclad PDLLA fiber [20]. After nearly 18 hours of immersion, the M1 fiber was still operational and capable of guiding light with IIL values of 1.3–1.35 dB/cm at 633 nm, 0.9 dB/cm at 850 nm, and 0.76 dB/cm at 950 nm, as shown in Fig. 14.

As previously mentioned, both the in vitro degradation as well as the immersion induced loss of polyester-based fibers highly depend on the fiber dimensions but also on their internal structure. For mbioPOF M1, we deal with a water penetrable microstructured fiber. Additionally, M1 has a diameter twice as small compared to the previously studied unclad PDLLA fibers (d = 588 μm) [20] and SI bioPOFs (d = 497 μm) [21]. Owing to that, the bulk degradation of microstructured PDLLA fiber is substantially delayed in comparison with the previously tested fibers. Given the above, we can anticipate on employing mbioPOFs as implantable fiber for various biomedical applications including PDT, or optogenetics, where the manipulation of the neural activity could be performed even over a 24 h activity following the timing of the biological events governed by the circadian clock [45]; or NIR-light activated controlled drug release typically applied in cancer therapy that enables on-demand, spatiotemporally controlled delivery of therapeutic agents in the time frame varying from only 30 minutes [46] to a few hours during which the decomposition of nanocarriers is required [47].

VII. Summary and Conclusion

We have reported on the fabrication and on the characterization of novel biodegradable microstructured polymer optical fibers (mbioPOFs), fabricated from commercially available amorphous polyester PDLLA, which is an FDA-regulated material.

First, we have described the optical simulations required to examine the confinement loss in mbioPOFs and the eventual design of the microstructure according to which we intended to fabricate the fibers. Subsequently, we have reported on the manufacturing of structured mbioPOF preforms with one ring and two rings of airholes using an entirely novel fabrication technique based on a specialty transfer-molding system, and we have explained how these preforms were drawn into actual mbioPOFs. We have found that all the fabricated mbioPOFs feature deviations from the intended geometry. We obtained fibers M1 and M2a, with diameters of 400 μm down to 200 μm, which displayed hole shrinkage and a larger pitch, whilst fiber M2b with a 100 μm diameter displayed airhole expansion and shape deformation. The mode confinement was therefore not as expected for both M1 and M2a fibers, but we obtained excellent mode confinement in fiber M2b, which corresponds to the first demonstration of geometry-based instead of refractive index difference-based optical waveguiding in a biocompatible and biodegradable polymer optical fiber.

From all the fabricated mbioPOFs, we found the lowest attenuation in fiber M1, which primarily results from the quality of

the preform. We obtained the lowest attenuation of 0.065 dB/cm for this fiber with a diameter d = 219 ± 27 μm, at a wavelength of 898 nm. We registered an attenuation of around 0.1 dB/cm in the range 750–980 nm for the same fiber. We also recorded attenuation values of 0.43 dB/cm and 0.50 dB/cm at 1580 nm for fiber M1 with outer diameters of d = 260 μm and d = 360 μm, respectively. These attenuation values represent a record low loss reported so far for biodegradable and biocompatible polymer optical fibers, both in the VIS and NIR range.

We have also shown that our mbioPOFs are truly degradable as supported by in vitro degradation studies of fibers with an average diameter of around 400, 200 and 100 μm. Their molar mass decreased down to 21, 25 and 43% of the original values after 105 days of incubation in PBS at 37 °C. All the mbioPOFs degrade at a slower rate than unclad PDLLA fibers due to the presence of the capillaries, and they also feature a considerably longer operational time from the optical standpoint, i.e., around 17 hours once the fibers are immersed in PBS at 37 °C. The immersion induced loss of fiber M1 after 6 h is below 0.5 dB/cm in the VIS range and 0.3 dB/cm in the NIR region.

Given these results, we can compare the merits of this new mbioPOF with those of our previously reported SI [21] and unclad bioPOFs [20]. First, our mbioPOF features lower optical loss than SI bioPOF. Note however, that the attenuation coefficient values vary essentially due to the different material properties, i.e., in the SI bioPOF the light is guided in a PDLGA core, whilst it is guided in PDLLA in our mbioPOF. Furthermore, the different preform fabrication methods also influence the optical loss. Second, our microstructured PDLLA-based optical fiber features slower *in-vitro* degradation and an extended operational time when immersed in a simulated biological environment compared to our previously reported SI bioPOF and unclad PDLLA fiber.

The excellent optical properties and the potential for achieving controllable degradation rates of mbioPOFs allow anticipating on their use as fully-fledged implantable optical fibers for deep tissue light delivery and on their application in biosensing or optogenetics, for which the optical functionalities must be maintained over a prolonged period of time.

Acknowledgment

The authors would like to thank Prof. Jürgen Van Erps and Prof. Michael Vervaeke from the B-PHOT research group at Vrije Universiteit Brussel for their assistance with the design of the polymer transfer molding processing tool. The authors also acknowledge the support of Bernhard De Meyer from the Polymer Chemistry and Biomaterials Group from Ghent University, who carried out the GPC measurements.

References

[1] A. Gierej, T. Geernaert, S. Van Vlierberghe, P. Dubruel, H. Thienpont, and F. Berghmans, "Challenges in the fabrication of biodegradable and implantable optical fibers for biomedical applications," *Mater.,* vol. 14, no. 1972, pp. 1–23, 2021, doi: 10.3390/ma14081972.

[2] A. Dupuis et al., "Prospective for biodegradable microstructured optical fibers," *Opt. Lett.*, vol. 32, no. 2, pp. 109–111, 2007, doi: 10.1364/OL.32.000109.

[3] S. T. Parker et al., "Biocompatible silk printed optical waveguides," *Adv. Mater.*, vol. 21, no. 23, pp. 2411–2415, 2009, doi: 10.1002/adma.200801580.

[4] M. B. Applegate, G. Perotto, D. L. Kaplan, and F. G. Omenetto, "Biocompatible silk step-index optical waveguides," *Biomed. Opt. Exp.*, vol. 6, no. 11, pp. 4221–4227, 2015, doi: 10.1364/BOE.6.004221.

[5] K. Hey Tow, D. M. Chow, F. Vollrath, I. Dicaire, T. Gheysens, and L. Thevenaz, "Exploring the use of native spider silk as an optical fiber for chemical sensing," *J. Lightw. Technol.*, vol. 36, no. 4, pp. 1138–1144, 2018, doi: 10.1109/JLT.2017.2756095.

[6] X. Qiao et al., "Synthetic engineering of spider silk fiber as implantable optical waveguides for low-loss light guiding," *ACS Appl. Mater. Interfaces*, vol. 9, pp. 14665–14676, 2017.

[7] A. Dupuis et al., "Fabrication strategies and potential applications of the "green" microstructured optical fibers," *J. Biomed. Opt.*, vol. 13, no. 5. pp. 1–5, 2008, doi: 10.1117/1.2978062.

[8] A. Dupuis et al., "Biodegradable, double-core, porous optical fiber for sensing applications," in *Proc. Opt. Fiber Sensors*, 2006, pp. 6–8.

[9] H. Orelma et al., "Optical cellulose fiber made from regenerated cellulose and cellulose acetate for water sensor applications," *Cellulose*, vol. 27, no. 3, pp. 1543–1553, 2020, doi: 10.1007/s10570-019-02882-3.

[10] A. Jain, A. H. J. Yang, and D. Erickson, "Gel-based optical waveguides with live cell encapsulation and integrated microfluidics," *Opt. Lett.*, vol. 37, pp. 1472–1474, 2012, doi: 10.1364/ol.37.001472.

[11] E. Fujiwara, T. D. Cabral, M. Sato, H. Oku, and C. M. B. Cordeiro, "Agarose-based structured optical fibre," *Sci. Rep.*, vol. 10, pp. 1–8, 2020, doi: 10.1038/s41598-020-64103-3.

[12] A. K. Manocchi, P. Domachuk, and F. G. Omenetto, "Facile fabrication of gelatin-based biopolymeric optical waveguides," *Biotechnol. Bioeng.*, vol. 103, no. 4, pp. 725–732, 2009.

[13] M. Choi, J. W. Choi, S. Kim, S. Nizamoglu, S. K. Hahn, and S. H. Yun, "Light-guiding hydrogels for cell-based sensing and optogenetic synthesis in vivo," *Nature Photon.*, vol. 7, no. 12, pp. 987–994, 2013, doi: 10.1038/nphoton.2013.278.

[14] M. Choi, M. Humar, S. Kim, and S. H. Yun, "Step-index optical fiber made of biocompatible hydrogels," *Adv. Mater.*, vol. 27, pp. 4081–4086, 2015, doi: 10.1002/adma.201501603.

[15] J. Guo et al., "Highly stretchable, strain sensing hydrogel optical fibers," *Adv. Mater.*, vol. 28, no. 46, pp. 10244–10249, 2016, doi: 10.1002/adma.201603160.

[16] A. K. Yetisen et al., "Glucose-sensitive hydrogel optical fibers functionalized with phenylboronic acid," *Adv. Mater.*, vol. 29, no. 15, 2017, Art. no. 1606380, doi: 10.1002/adma.201606380.

[17] R. Fu, W. Luo, R. Nazempour, D. Tan, H. Ding, and K. Zhang, "Implantable and biodegradable poly (L-lactic acid) fibers for optical neural interfaces," *Adv. Opt. Mater.*, vol. 6, no. 3, pp. 1–8, 2017, doi: 10.1002/adom.201700941.

[18] S. Nizamoglu et al., "Bioabsorbable polymer optical waveguides for deep-tissue photomedicine," *Nature Commun.*, vol. 7, no. 1, pp. 1–7, 2016, doi: 10.1038/ncomms10374.

[19] D. Shan et al., "Flexible biodegradable citrate-based polymeric step-index optical fiber," *Biomaterials*, vol. 143, pp. 142–148, 2017, doi: 10.1016/j.biomaterials.2017.08.003.

[20] A. Gierej et al, "Poly(D, L-Lactic acid) (PDLLA) biodegradable and biocompatible polymer optical fiber," *J. Lightw. Technol.*, vol. 37, no. 9, pp. 1916–1923, May 2019, doi: 10.1109/JLT.2019.2895220.

[21] A. Gierej et al., "On the characterization of novel step-index biocompatible and biodegradable poly(D, L-lactic acid) based optical fiber," *J. Lightw. Technol.*, vol. 38, no. 7, pp. 1905–1914, Apr. 2019, doi: 10.1109/jlt.2019.2959945.

[22] S. Shadman et al., "Microstructured biodegradable fibers for advanced control delivery," *Adv. Funct. Mater.*, vol. 30, 2020, Art. no. 1910283, doi: 10.1002/adfm.201910283.

[23] E. Ceci-Ginistrelli et al., "Novel biocompatible and resorbable UV-transparent phosphate glass based optical fiber," *Opt. Mater. Exp.*, vol. 6, no. 6, pp. 2040–2051, 2016, doi: 10.1364/OME.6.002040.

[24] A. Mishra, F. Désévédavy, L. Petit, F. Smektala, and J. Massera, "Core-clad phosphate glass fibers for biosensing," *Mater. Sci. Eng.: C*, vol. 96, pp. 458–465, 2018, doi: 10.1016/j.msec.2018.11.038.

[25] D. Gallichi-Nottiani, D. Pugliese, N. G. Boetti, D. Milanese, and D. Janner, "Toward the fabrication of extruded microstructured bioresorbable phosphate glass optical fibers," *Int. J. Appl. Glass Sci.*, vol. 11, pp. 632–640, 2019, doi: 10.1111/ijag.14652.

[26] D. Pugliese et al., "Bioresorbable optical fiber Bragg gratings," *Opt. Lett.*, vol. 43, no. 4, pp. 671–674, 2018, doi: 10.1364/OL.43.000671.
[27] S. Park et al., "One-step optogenetics with multifunctional flexible polymer fibers," *Nature Neurosci.*, vol. 20, no. 4, pp. 612–619, 2017, doi: 10.1038/nn.4510.
[28] C. Faccini de Lima, L. A. van der Elst, V. N. Koraganji, M. Zheng, M. G. Kurtoglu, and A. Gumennik, "Towards digital manufacturing of smart multimaterial fibers," *Nanoscale Res. Lett.*, vol. 14, pp. 1–6, 2019, doi: 10.1186/s11671-019-3031-x.
[29] A. Kilias, A. Canales, U. P. Froriep, S. Park, U. Egert, and P. Anikeeva, "Optogenetic entrainment of neural oscillations with hybrid fiber probes," *J. Neural Eng.*, vol. 15, no. 5, Oct. 2018, Art. no. 56006, doi: 10.1088/1741-2552/aacdb9.
[30] D. Pysz et al., "Stack and draw fabrication of soft glass microstructured fiber optics," *Bull. Polish Acad. Sci. Tech. Sci.*, vol. 62, no. 4, pp. 667–682, 2014, doi: 10.2478/bpasts-2014-0073.
[31] T. A. Birks, J. C. Knight, and P. S. J. Russell, "Endlessly single-mode photonic crystal fiber," *Opt. Lett.*, vol. 22, no. 13, pp. 961–963, 1997.
[32] P. Russel, "Photonic crystal fibers," *Science*, vol. 299, pp. 358–362, 2003, doi: 10.1126/science.1079280.
[33] J. M. Dudley, G. Genty, and S. Coen, "Supercontinuum generation in photonic crystal fiber," *Rev. Modern Phys.*, vol. 78, pp. 1135–1184, 2006, doi: 10.1103/RevModPhys.78.1135.
[34] M. A. van Eijkelenborg et al., "Microstructured polymer optical fibre," *Opt. Exp.*, vol. 9, no. 7, pp. 319–327, 2001, doi: 10.1109/ofc.2002.1036532.
[35] M. C. J. Large, L. Poladian, G. W. Barton, and M. A. van Eijkelenborg, *Microstructured Polymer Optical Fibres*. Berlin, Germany: Springer, 2007.
[36] A. Argyros, "Microstructured polymer optical fibers," *J. Lightw. Technol.*, vol. 27, no. 11, pp. 1571–1579, Jun. 2009, doi: 10.1109/JLT.2009.2020609.
[37] U. S. Food and Drug Administration, "Drug master files (DMFs)." Accessed: Sep. 12, 2022. [Online]. Available: https://www.fda.gov/media/159995/download
[38] Corbion, "Polymers for medical devices," 2018. Accessed: Jul. 30, 2018. [Online]. Available: https://www.corbion.com/static/downloads/datasheets/30d/PURASORBPDL20.pdf
[39] L. Inc., "Lumerical MODE." Accessed: Sep. 12, 2022. [Online]. Available: https://www.lumerical.com/products/mode/
[40] B. H. Stuart, *Infrared Spectroscopy: Fundamentals and Applications*. Chichester, West Sussex, England: Wiley, 2004, doi: 10.1002/0470011149.
[41] E. Meaurio, E. Zuza, N. López-Rodríguez, and J. R. Sarasua, "Conformational behavior of poly($_{\mathrm{L}}$-lactide) studied by infrared spectroscopy," *J. Phys. Chem. B*, vol. 110, no. 11, pp. 5790–5800, Mar. 2006, doi: 10.1021/jp055203u.
[42] A. Skumanich, M. Jurich, and J. D. Swalen, "Absorption and scattering in nonlinear optical polymeric systems," *Appl. Phys. Lett.*, vol. 62, no. 5, pp. 446–448, 1993, doi: 10.1063/1.109618.
[43] E. J. Rodriguez, B. Marcos, and M. A. Huneault, "Hydrolysis of polylactide in aqueous media," *J. Appl. Polym. Sci.*, vol. 133, no. 44, pp. 1–11, 2016, doi: 10.1002/app.44152.
[44] I. Grizzi, H. Garreau, S. Li, and M. Vert, "Hydrolytic degradation of devices based on poly($_{\mathrm{DL}}$-lactic acid) size-dependence," *Biomaterials*, vol. 16, no. 4, pp. 305–311, 1995, doi: 10.1016/0142-9612(95)93258-F.
[45] M. M. Sidor and C. A. McClung, "Timing matters: Using optogenetics to chronically manipulate neural circuitry and rhythms," *Front. Behav. Neurosci.*, vol. 8, pp. 1–7, 2014, doi: 10.3389/fnbeh.2014.00041.
[46] J. Su et al., "Bioinspired nanoparticles with NIR-Controlled drug release for synergetic chemophotothermal therapy of metastatic breast cancer," *Adv. Funct. Mater.*, vol. 26, no. 41, pp. 7495–7506, 2016, doi: 10.1002/adfm.201603381.
[47] T. Zhao et al., "Near-infrared triggered decomposition of nanocapsules with high tumor accumulation and stimuli responsive fast elimination," *Angewandte Chemie*, vol. 130, no. 10, pp. 2641–2645, 2018, doi: 10.1002/ange.201711354.